

# Unequal-arm Interferometry and Ranging in Space

Massimo Tinto\*

*Jet Propulsion Laboratory, California Institute of Technology, Pasadena, CA 91109*

(Dated: December 12, 2005)

## Abstract

Space-borne interferometric gravitational wave detectors, sensitive in the low-frequency (milli-hertz) band, will fly in the next decade. In these detectors the spacecraft-to-spacecraft light-travel-times will necessarily be unequal, time-varying, and (due to aberration) have different time delays on up- and down-links. By using knowledge of the inter-spacecraft light-travel-times and their time evolution it is possible to cancel in post-processing the otherwise dominant laser phase noise and obtain a variety of interferometric data combinations sensitive to gravitational radiation. This technique, which has been named Time-Delay Interferometry (TDI), can be implemented with constellations of three or more formation-flying spacecraft that coherently track each other. As an example application we consider the Laser Interferometer Space Antenna (LISA) mission and show that TDI combinations can be synthesized by properly time-shifting and linearly combining the phase measurements performed on board the three spacecraft. Since TDI exactly suppresses the laser noises when the delays coincide with the light-travel-times, we then show that TDI can also be used for estimating the time-delays needed for its implementation. This is done by performing a post-processing non-linear minimization procedure, which provides an effective, powerful, and simple way for making measurements of the inter-spacecraft light-travel-times. This processing technique, named Time-Delay Interferometric Ranging (TDIR), is highly accurate in estimating the time-delays and allows TDI to be successfully implemented without the need of a dedicated ranging subsystem.

PACS numbers:

---

\*Electronic address: [Massimo.Tinto@jpl.nasa.gov](mailto:Massimo.Tinto@jpl.nasa.gov); Also at: LIGO Laboratories, California Institute of Technology, Pasadena, CA 91125

## I. INTRODUCTION

Interferometric detectors of gravitational radiation (with frequency content  $0 < f < f_u$ ) use a coherent train of electromagnetic waves (of nominal frequency  $\nu_0 \gg f_u$ ) folded into several beams, and at one or more points where these intersect, monitor relative fluctuations of frequency or phase (homodyne detection). The observed low frequency fluctuations are due to several causes: (a) frequency variations of the source of the electromagnetic signal about  $\nu_0$ , (b) relative motions of the electromagnetic source and the mirrors (or amplifying transponders) that do the folding, (c) temporal variations of the index of refraction along the beams, and, (d) according to general relativity, to any time-variable gravitational fields present, such as the transverse-traceless metric curvature of a passing plane gravitational wave (GW). To observe gravitational waves in this way, it is thus necessary to control, or monitor, the other sources of relative frequency fluctuations, and, in the data analysis, to use optimal algorithms based on the different characteristic interferometer responses to gravitational waves (the signal) and to the other sources (the noise) [1]. By comparing phases of electromagnetic beams referenced to the same frequency generator and propagated along non-parallel equal-length arms, frequency fluctuations of the frequency reference can be removed and gravitational wave signals at levels many orders of magnitude lower can be detected.

In the present single-spacecraft Doppler tracking observations, for instance, many of the noise sources can be either reduced or calibrated by implementing appropriate microwave frequency links and by using specialized electronics [2], so the fundamental limitation is imposed by the frequency (time-keeping) fluctuations inherent to the reference clock that controls the microwave system. Hydrogen maser clocks, currently used in Doppler tracking experiments, achieve their best performance at about 1000 seconds integration time, with a fractional frequency stability of a few parts in  $10^{-16}$ . This is the reason why these one-arm interferometers in space (which have one Doppler readout and a "3-pulse" response to gravitational waves [3]) are most sensitive to millihertz gravitational waves. This integration time is also comparable to the microwave propagation (or "storage") time  $2L/c$  to spacecraft en route to the outer solar system (for example  $L \simeq 5 - 8$  AU for the Cassini spacecraft) [2].

Next-generation low-frequency interferometric gravitational wave detectors in solar orbits, such as the Laser Interferometer Space Antenna (LISA) mission [4] and the Astrodynamical

Space Test of Relativity using Optical Devices (ASTROD) mission [5], have been proposed to achieve greater sensitivity to millihertz gravitational waves. Since the armlengths of these space-based interferometers can differ by a few percent (for LISA) to tens of percents (for ASTROD), the direct recombination of the two beams at a photo detector will not effectively remove the laser frequency noise. This is because the frequency fluctuations of the laser will be delayed by different amounts within the two unequal length arms. In order to cancel the laser frequency noise, the time-varying Doppler data must be recorded and post-processed to allow for arm-length differences [6]. The data streams will have temporal structure, which can be described as due to many-pulse responses to  $\delta$ -function excitations, depending on time-of-flight delays in the response functions of the instrumental Doppler noises and in the response to incident plane-parallel, transverse, and traceless gravitational waves.

In what follows we will give an account of TDI as it will be implemented by LISA. Each of its three spacecraft orbiting the sun will be equipped with two lasers sending beams to the other two ( $\sim 0.03$  AU away) while simultaneously measuring the beat frequencies between the local laser and the laser beams received from the other spacecraft. The description of TDI that will be presented in this article will assume a successful prior removal of any first-order Doppler beat notes due to spacecraft relative motions [7], giving six residual inter-spacecraft Doppler time series as the raw data of a *stationary* time delay space interferometer. Following [8], [9], [10], we will regard LISA not as constituting one or more conventional Michelson interferometers, but rather, in a symmetrical way, a closed array of six one-arm delay lines between the test masses. This point of view is very powerful since it allows one to synthesize new data combinations that cancel laser frequency noises, and estimate achievable sensitivities of these combinations in terms of the separate and relatively simple single arm-responses both to gravitational wave and instrumental noise.

In contrast to Earth-based interferometers, which operate in the long-wavelength limit (LWL) (arm lengths  $\ll$  gravitational wavelength  $\sim c/f_0$ , where  $f_0$  is a characteristic frequency of the GW), LISA will *not* operate in the LWL over much of its frequency band. When the physical scale of a free mass optical interferometer intended to detect gravitational waves is comparable to or larger than the GW wavelength, time delays in the response of the instrument to the waves, and travel times along beams in the instrument, cannot be ignored and must be allowed for in computing the detector response used for data interpretation.

This article is organized as follows. In Section II we summarize the one-arm Doppler

transfer functions of an optical beam between two carefully shielded test masses inside each spacecraft resulting from (i) frequency fluctuations of the lasers used in transmission and reception, (ii) fluctuations due to non-inertial motions of the spacecraft, (iii) beam-pointing fluctuations and shot noise [11]. Among these, the dominant noise is from the frequency fluctuations of the lasers and is several orders (perhaps 7 or 8) above the other noises. This noise must be very precisely removed from the data in order to achieve the GW sensitivity at the level set by the remaining Doppler noise sources, which are at a much lower level and constitute the noise floor after the laser frequency noise is suppressed. We show that this can be accomplished by shifting and linearly combining the twelve one-way Doppler data LISA will measure. The actual procedure can easily be understood in terms of properly defined time-delay operators that act on the one-way Doppler measurements.

As an example application, we then derive the unequal-arm Michelson interferometric combination in the simple case in which the light-travel-times are constant in time and independent from being up- or down-links. The expressions for the Sagnac interferometric combinations,  $(\alpha, \beta, \gamma, \zeta)$  as well as all those combinations that rely only on four of the possible six inter-spacecraft Doppler measurements (denoted  $P$ ,  $E$  and  $U$ ) are not derived in this article, and the reader is referred to [12, 13] for details on their derivations.

In Section III we then consider the formulation of TDI when spacecraft-to-spacecraft light-travel-times are not constant in time, and dependent from being up- or down-links. Reduction of data from moving interferometric laser arrays in solar orbit will in fact encounter non-symmetric up- and downlink light time differences that are significant, and need to be accounted for in order to exactly cancel the laser frequency fluctuations [12, 14, 15]. In Section IV we show that, by introducing a set of non-commuting time-delay operators, there exists a quite general procedure for deriving generalized TDI combinations that account for the effects of time-dependence of the arms. Using this approach it is possible to derive “flex-free” expression for the unequal-arm Michelson combinations  $X_1$ , and obtain the generalized expressions for all the TDI observables [13].

Since TDI relies on the accurate knowledge of the time-delays that have to be applied to the phase measurements, in Section IV we show that it is possible to estimate the delays by implementing a non-linear least-squares minimization procedure in which a TDI combination is used for estimating the time-delays. This procedure, which has been called Time-Delay Interferometric Ranging (TDIR) [16], relies on the fact that TDI nulls all the laser noises

when the time delays are chosen to match the travel times experienced by the laser beams as they propagate along the sides of the array. TDIR allows the implementation of TDI without a separate inter-spacecraft ranging subsystem, significantly simplifying the design of the LISA instrument. At the very least, TDIR can supplement such a subsystem, allowing the synthesis of TDI combinations during ranging dropouts or glitches.

## II. TIME-DELAY INTERFEROMETRY (TDI)

### A. Statement of the Problem

Equal-arm interferometer detectors of gravitational waves can observe gravitational radiation by canceling the laser frequency fluctuations affecting the light injected into their arms. This is done by comparing phases of split beams propagated along the equal (but non-parallel) arms of the detector. The laser frequency fluctuations affecting the two beams experience the same delay within the two equal-length arms and cancel out at the photodetector where relative phases are measured. This way gravitational wave signals of dimensionless amplitude less than  $10^{-20}$  can be observed when using lasers whose frequency stability can be as large as roughly a few parts in  $10^{-13}$ .

If the arms of the interferometer have different lengths, however, the exact cancellation of the laser frequency fluctuations, say  $C(t)$ , will no longer take place at the photodetector. In fact, the larger the difference between the two arms, the larger will be the magnitude of the laser frequency fluctuations affecting the detector response. If  $L_1$  and  $L_2$  are the lengths of the two arms, it is easy to see that the amount of laser relative frequency fluctuations remaining in the response is equal to (units in which the speed of light  $c = 1$ )

$$\Delta C(t) = C(t - 2L_1) - C(t - 2L_2) . \quad (1)$$

In the case of LISA, whose lasers are expected to display relative frequency fluctuations equal to about  $10^{-13}/\sqrt{Hz}$  in the millihertz band, and whose arms will differ by a few percent [4], equation (1) implies the following expression for the amplitude of the Fourier components of the uncanceled laser frequency fluctuations (an over imposed tilde denotes the operation of Fourier transform)

$$|\widetilde{\Delta C}(f)| \simeq |\widetilde{C}(f)| 4\pi f |L_1 - L_2| . \quad (2)$$

At  $f = 10^{-3}$  Hz, for instance, and assuming  $|L_1 - L_2| \simeq 0.5$  sec, the uncanceled fluctuations from the laser are equal to  $6.3 \times 10^{-16}/\sqrt{\text{Hz}}$ . Since the LISA sensitivity goal is about  $10^{-20}/\sqrt{\text{Hz}}$  in this part of the frequency band, it is clear that an alternative experimental approach for canceling the laser frequency fluctuations is needed.

The solution to this problem can be understood through Figure 1. In this idealized model the two beams exiting the two arms are not made to interfere at a common photodetector. Rather, each is made to interfere with the incoming light from the laser at a photodetector, decoupling in this way the phase fluctuations experienced by the two beams in the two arms. Now two Doppler measurements are available in digital form, and the problem becomes one of identifying an algorithm for digitally canceling the laser frequency fluctuations from a resulting new data combination.

The algorithm that performs the cancellation of the laser noise from the two Doppler measurements from the two arms, say  $y_1(t)$  and  $y_2(t)$ , works as follows. Let us denote with  $h_1(t)$ ,  $h_2(t)$  the gravitational wave signals entering into the Doppler data  $y_1$ ,  $y_2$  respectively, and with  $n_1$ ,  $n_2$  any other remaining noise affecting  $y_1$  and  $y_2$  respectively. The resulting expressions for the Doppler observables  $y_1$ ,  $y_2$  can be written in the following form

$$y_1(t) = C(t - 2L_1) - C(t) + h_1(t) + n_1(t) , \quad (3)$$

$$y_2(t) = C(t - 2L_2) - C(t) + h_2(t) + n_2(t) . \quad (4)$$

From Eqs. (3, 4) it is important to note the characteristic time signature of the random process  $C(t)$  in the Doppler responses  $y_1$ ,  $y_2$ . The time signature of the noise  $C(t)$  in  $y_1(t)$ , for instance, can be understood by observing that the frequency of the signal received at time  $t$  contains laser frequency fluctuations transmitted  $2L_1$  seconds earlier. By subtracting from the frequency of the received signal the frequency of the signal transmitted at time  $t$ , we also subtract the frequency fluctuations  $C(t)$  with the net result shown in Eq. (3).

From Eqs.(3, 4) we may notice that, by taking the difference of the two Doppler data  $y_1(t)$ ,  $y_2(t)$ , the frequency fluctuations of the laser enter into this new data set in the following way

$$y_1(t) - y_2(t) = C(t - 2L_1) - C(t - 2L_2) + h_1(t) - h_2(t) + n_1(t) - n_2(t) . \quad (5)$$

If we now compare how the laser frequency fluctuations enter into Eq. (5) against how they appear in Eqs. (3, 4) we can further make the following observation. If we time-shift the data  $y_1(t)$  by the round trip light time in arm 2,  $y_1(t - 2L_2)$ , and subtract from it the data

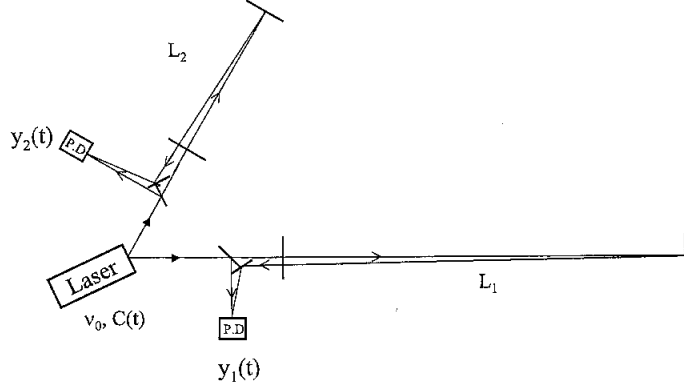


FIG. 1: Light from a laser is split into two beams, each injected into an arm formed by pairs of free-falling mirrors. Since the length of the two arms,  $L_1$  and  $L_2$ , are different, the light beams from the two arms are not recombined at one photo detector. Instead each is separately made to interfere with the light that is injected into the arms. Two distinct photo detectors are used, and phase (or frequency) fluctuations are then monitored and recorded there.

$y_2(t)$  after it has been time-shifted by the round trip light time in arm 1,  $y_2(t - 2L_1)$ , we obtain the following data set

$$\begin{aligned}
 y_1(t - 2L_2) - y_2(t - 2L_1) &= C(t - 2L_1) - C(t - 2L_2) + h_1(t - 2L_2) - h_2(t - 2L_1) \\
 &\quad + n_1(t - 2L_2) - n_2(t - 2L_1) .
 \end{aligned} \tag{6}$$

In other words, the laser frequency fluctuations enter into  $y_1(t) - y_2(t)$ , and  $y_1(t - 2L_2) - y_2(t - 2L_1)$  with the same time structure. This implies that, by subtracting Eq. (6) from Eq.

(5) we can generate a new data set that does not contain the laser frequency fluctuations  $C(t)$

$$X \equiv [y_1(t) - y_2(t)] - [y_1(t - 2L_2) - y_2(t - 2L_1)] . \quad (7)$$

The expression above of the  $X$  combination shows that it is possible to cancel the laser frequency noise in the time domain by properly time-shifting and linearly combining Doppler measurements recorded by different Doppler readouts. This in essence is what TDI amounts to. In what follows we will further elaborate and generalize TDI to the realistic LISA configuration.

## B. TDI

The description of TDI for LISA is greatly simplified if we adopt the notation shown in Figure 2 , where the overall geometry of the LISA detector is defined. There are three spacecraft, six optical benches, six lasers, six proof-masses and twelve photodetectors. There are also six phase difference data going clock-wise and counter-clockwise around the LISA triangle. For the moment we will make the simplifying assumption that the array is stationary, i.e. the back and forth optical paths between pairs of spacecraft are simply equal to their relative distances [12–15].

The spacecraft are labeled 1, 2, 3 and their separating distances are denoted  $L_1, L_2, L_3$ , with  $L_i$  being opposite spacecraft  $i$ . We orient the vertices 1, 2, 3 clockwise in figure 2. Unit vectors between spacecraft are  $\hat{n}_i$ , oriented as indicated in figure 2. We index the phase difference data to be analyzed as follows: the beam arriving at spacecraft  $i$ , transmitted by spacecraft  $j$  gives rise to the phase measurement  $s_{ji}$  (along  $L_k$ ). Similarly,  $s_{ij}$  is the phase difference series derived from reception at spacecraft  $j$  with transmission from spacecraft  $i$ . The other four one-way phase difference time series from signals exchanged between the spacecraft are obtained by cyclic permutation of the indices:  $1 \rightarrow 2 \rightarrow 3 \rightarrow 1$ . We also adopt a notation for delayed data streams, which will be convenient later for algebraic manipulations. We define the three time-delay operators  $\mathcal{D}_i$ ,  $i = 1, 2, 3$  where for any data stream  $x(t)$ ,

$$\mathcal{D}_i x(t) \equiv x(t - L_i) , \quad (8)$$

where  $L_i, i = 1, 2, 3$  are the light travel times along the three arms of the LISA triangle (the speed of light  $c$  is assumed to be unity in this article). Thus, for example,

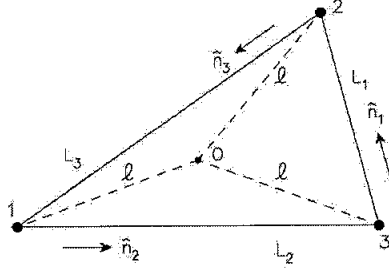


FIG. 2: Schematic LISA configuration. The spacecraft are labeled 1, 2, and 3. The optical paths are denoted by  $L_i$ , where the index  $i$  corresponds to the opposite spacecraft. The unit vectors  $\hat{n}_i$  point between pairs of spacecraft, with the orientation indicated.

$\mathcal{D}_2 s_{13}(t) = s_{13}(t - L_2)$ ,  $\mathcal{D}_2 \mathcal{D}_3 s_{13}(t) = s_{13}(t - L_2 - L_3) = \mathcal{D}_3 \mathcal{D}_2 s_{13}(t)$ , etc. Note that the operators commute here. This is because the arm-lengths have been assumed to be constant in time. If the  $L_i$  are functions of time then the operators no longer commute [12, 13, 15], as will be described later.

Six more phase difference series result from laser beams exchanged between adjacent optical benches within each spacecraft; these are similarly indexed as  $\tau_{ij}$ ,  $i, j = 1, 2, 3, i \neq j$ . The proof-mass-plus-optical-bench assemblies for LISA spacecraft number 1 are shown schematically in figure 3. The photo receivers that generate the data  $s_{21}$ ,  $s_{31}$ ,  $\tau_{21}$ , and  $\tau_{31}$  at spacecraft 1 are shown. The phase fluctuations from the six lasers, which need to be canceled, can be represented by six random processes  $p_i, p_i^*$ , where  $p_i, p_i^*$  are the phases of the lasers in spacecraft  $i$  on the left and right optical benches respectively as shown in the figure. We extend the cyclic terminology so that at vertex  $i$  ( $i = 1, 2, 3$ ) the random displacement vectors of the two proof masses are respectively denoted by  $\vec{\delta}_i(t), \vec{\delta}_i^*(t)$ , and the random displacements (perhaps several orders of magnitude greater) of their optical benches are correspondingly denoted by  $\vec{\Delta}_i(t), \vec{\Delta}_i^*(t)$  where a \* added to a quantity means that it is located on the right optical bench. As pointed out in [11], the analysis does not

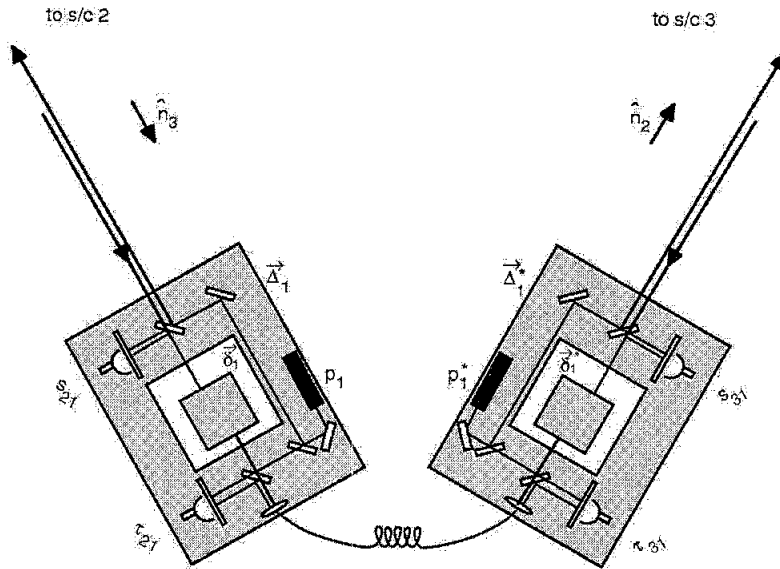


FIG. 3: Schematic diagram of proof-masses-plus-optical-benches for a LISA spacecraft. The left-hand bench reads out the phase signals  $s_{21}$  and  $\tau_{21}$ . The right hand bench analogously reads out  $s_{31}$  and  $\tau_{31}$ . The random displacements of the two proof masses and two optical benches are indicated (lower case  $\vec{\delta}_i, \vec{\delta}_i^*$  for the proof masses, upper case  $\vec{\Delta}_i, \vec{\Delta}_i^*$  for the optical benches).

assume that pairs of optical benches are rigidly connected, i.e.  $\vec{\Delta}_i \neq \vec{\Delta}_i^*$ , in general. The present LISA design shows optical fibers transmitting signals both ways between adjacent benches. We ignore time-delay effects for these signals and will simply denote by  $\mu_i(t)$  the phase fluctuations upon transmission through the fibers of the laser beams with frequencies  $\nu_i$ , and  $\nu_i^*$ . The  $\mu_i(t)$  phase shifts within a given spacecraft might not be the same for large frequency differences  $\nu_i - \nu_i^*$ . For the envisioned frequency differences (a few hundred megahertz), however, the remaining fluctuations due to the optical fiber can be neglected [11]. It is also assumed that the phase noise added by the fibers is independent of the direction of light propagation through them. For ease of presentation, in what follows we will assume the center frequencies of the lasers to be the same, and denote this frequency by  $\nu_0$ .

The laser phase noise in  $s_{23}$  is therefore equal to  $\mathcal{D}_1 p_2(t) - p_3^*(t)$ . Similarly, since  $s_{32}$  is the phase shift measured on arrival at spacecraft 2 along arm 1 of a signal transmitted from spacecraft 3, the laser phase noises enter into it with the following time signature:

$\mathcal{D}_1 p_3^*(t) - p_2(t)$ . Figure 3 endeavors to make the detailed light paths for these observations clear. An outgoing light beam transmitted to a distant spacecraft is routed from the laser on the local optical bench using mirrors and beam splitters; this beam does not interact with the local proof mass. Conversely, an *incoming* light beam from a distant spacecraft is bounced off the local proof mass before being reflected onto the photo receiver where it is mixed with light from the laser on that same optical bench. The inter-spacecraft phase data are denoted  $s_{21}$  and  $s_{31}$  in figure 3.

Beams between adjacent optical benches within a single spacecraft are bounced off proof masses in the opposite way. Light to be *transmitted* from the laser on an optical bench is *first* bounced off the proof mass it encloses and then directed to the other optical bench. Upon reception it does *not* interact with the proof mass there, but is directly mixed with local laser light, and again down converted. These data are denoted  $\tau_{21}$  and  $\tau_{31}$  in figure 3.

The expressions for the  $s_{ji}$  and  $\tau_{ji}$  phase measurements can now be developed from figures 2 and 3, and they are for the particular LISA configuration in which all the lasers have the same nominal frequency  $\nu_0$ , and the spacecraft are stationary with respect to each other. Consider the  $s_{31}(t)$  process (equation (11) below). The photo receiver on the right bench of spacecraft 1, which (in the spacecraft frame) experiences a time-varying displacement  $\vec{\Delta}_1^*$ , measures the phase difference  $s_{31}$  by first mixing the beam from the distant optical bench 3 in direction  $\hat{n}_2$ , and laser phase noise  $p_3$  and optical bench motion  $\vec{\Delta}_3$  that have been delayed by propagation along  $L_2$ , after one bounce off the proof mass ( $\vec{\delta}_1^*$ ), with the local laser light (with phase noise  $p_1^*$ ). Since for this simplified configuration no frequency offsets are present, there is of course no need for any heterodyne conversion [7].

In equation (10) the  $\tau_{21}$  measurement results from light originating at the right-bench laser ( $p_1^*$ ,  $\vec{\Delta}_1^*$ ), bounced once off the right proof mass ( $\vec{\delta}_1^*$ ), and directed through the fiber (incurring phase shift  $\mu_1(t)$ ), to the left bench, where it is mixed with laser light ( $p_1$ ). Similarly the right bench records the phase differences  $s_{31}$  and  $\tau_{31}$ . The laser noises, the gravitational wave signals, the optical path noises, and proof-mass and bench noises, enter into the four data streams recorded at vertex 1 according to the following expressions [11]:

$$s_{21} = s_{21}^{\text{gw}} + s_{21}^{\text{opt. path}} + \mathcal{D}_3 p_2^* - p_1 + \nu_0 \left[ -2\hat{n}_3 \cdot \vec{\delta}_1 + \hat{n}_3 \cdot \vec{\Delta}_1 + \hat{n}_3 \cdot \mathcal{D}_3 \vec{\Delta}_2^* \right], \quad (9)$$

$$\tau_{21} = p_1^* - p_1 - 2 \nu_0 \hat{n}_2 \cdot (\vec{\delta}_1^* - \vec{\Delta}_1^*) + \mu_1. \quad (10)$$

$$s_{31} = s_{31}^{\text{gw}} + s_{31}^{\text{opt. path}} + \mathcal{D}_2 p_3 - p_1^* + \nu_0 \left[ 2\hat{n}_2 \cdot \vec{\delta}_1^* - \hat{n}_2 \cdot \vec{\Delta}_1^* - \hat{n}_2 \cdot \mathcal{D}_2 \vec{\Delta}_3 \right], \quad (11)$$

$$\tau_{31} = p_1 - p_1^* + 2 \nu_0 \hat{n}_3 \cdot (\vec{\delta}_1 - \vec{\Delta}_1) + \mu_1. \quad (12)$$

Eight other relations, for the readouts at vertices 2 and 3, are given by cyclic permutation of the indices in equations (9)-(12).

The gravitational wave phase signal components,  $s_{ji}^{\text{gw}}$  in equations (9) and (11) are given by integrating with respect to time equations (1), and (2) of reference [9], which relate metric perturbations to optical frequency shifts. The optical path phase noise contributions,  $s_{ij}^{\text{opt. path}}$ , which include shot noise from the low signal-to-noise ratio (SNR) in the links between the distant spacecraft, can be derived from the corresponding terms given in [11]. The  $\tau_{ij}$  measurements will be made with high SNR so that for them the shot noise is negligible.

In order to simplify the derivation of the expressions canceling the laser and optical bench noises, let us focus for the moment only on the laser and optical bench noises entering into the observables  $s_{ij}$  and  $\tau_{ij}$ . Note that by subtracting Eq.(12) from Eq. (10), we can rewrite the resulting expression (and those obtained from it by permutation of the spacecraft indices) in the following form,

$$z_1 \equiv \frac{1}{2}(\tau_{21} - \tau_{31}) = \phi_1^* - \phi_1, \quad (13)$$

where  $\phi_1^*$ ,  $\phi_1$  are defined as,

$$\begin{aligned} \phi_1^* &\equiv p_1^* + \nu_0 \hat{n}_2 \cdot \vec{\Delta}_1^*, \\ \phi_1 &\equiv p_1 - \nu_0 \hat{n}_3 \cdot \vec{\Delta}_1, \end{aligned} \quad (14)$$

The importance in defining these combinations is that the expressions for the data streams  $s_{ij}$  simplify into the following form,

$$\begin{aligned} s_{21} &= \mathcal{D}_3 \phi_2^* - \phi_1, \\ s_{31} &= \mathcal{D}_2 \phi_3 - \phi_1^*. \end{aligned} \quad (15)$$

If we now combine the  $s_{ij}$ , and  $z_i$  in the following way,

$$\eta_1 \equiv s_{21} - \mathcal{D}_3 z_2 = \mathcal{D}_3 \phi_2 - \phi_1, \quad \eta_{1*} \equiv s_{31} + z_1 = \mathcal{D}_2 \phi_3 - \phi_1, \quad (16)$$

$$\eta_2 \equiv s_{32} - \mathcal{D}_1 z_3 = \mathcal{D}_1 \phi_3 - \phi_2, \quad \eta_{2*} \equiv s_{12} + z_2 = \mathcal{D}_3 \phi_1 - \phi_2, \quad (17)$$

$$\eta_3 \equiv s_{13} - \mathcal{D}_2 z_1 = \mathcal{D}_2 \phi_1 - \phi_3, \quad \eta_{3*} \equiv s_{23} + z_3 = \mathcal{D}_1 \phi_2 - \phi_3, \quad (18)$$

we have just reduced the problem of canceling of six laser and six optical bench noises to the equivalent problem of removing the three random processes,  $\phi_1$ ,  $\phi_2$ , and  $\phi_3$ , from the six linear combinations,  $\eta_i$ ,  $\eta_i^*$ , of the one-way measurements  $s_{ij}$ , and  $z_i$ .

### C. The Unequal-arm Michelson Combination

In order to show how the delay operators can be used for deriving interferometric measurements, we will consider the simple case of the unequal-arm Michelson Interferometer combination  $X$ . This TDI combination relies on the four measurements  $\eta_1$ ,  $\eta_{1*}$ ,  $\eta_{2*}$ , and  $\eta_3$ . Note that the two combinations  $\eta_3 + \mathcal{D}_3 \eta_{2*}$ ,  $\eta_{1*} + \mathcal{D}_2 \eta_3$ , which represent the two synthesized two-way data measured onboard spacecraft 1, can be written in the following form

$$\eta_1 + \mathcal{D}_3 \eta_{2*} = (\mathcal{D}_3 \mathcal{D}_3 - I) \phi_1, \quad (19)$$

$$\eta_{1*} + \mathcal{D}_2 \eta_3 = (\mathcal{D}_2 \mathcal{D}_2 - I) \phi_1, \quad (20)$$

where  $I$  is the identity operator. Note that in the stationary case any pairs of these operators commute since up- and down- delays are equal. This in general is no longer true when the delays are functions of time).

From equations (19, 20) it is easy to derive the following expression for  $X$ , by requiring the elimination of  $\phi_1$

$$\begin{aligned} X &= [\mathcal{D}_2 \mathcal{D}_2 - I] (\eta_1 + \mathcal{D}_3 \eta_{2*}) - [(\mathcal{D}_3 \mathcal{D}_3 - I)] (\eta_{1*} + \mathcal{D}_2 \eta_3) \\ &= [(\eta_{1*} + \mathcal{D}_2 \eta_3) + \mathcal{D}_2 \mathcal{D}_2 (\eta_1 + \mathcal{D}_3 \eta_{2*})] - [(\eta_1 + \mathcal{D}_3 \eta_{2*}) + \mathcal{D}_3 \mathcal{D}_3 (\eta_{31} + \mathcal{D}_2 \eta_{13})] \end{aligned} \quad (21)$$

After replacing equations (16, 17, 18) into equation (21), we obtain the final expression for  $X$  valid in the case of a static LISA array

$$\begin{aligned} X &= [(s_{31} + \mathcal{D}_2 s_{13}) + \mathcal{D}_2 \mathcal{D}_2 (s_{21} + \mathcal{D}_3 s_{12})] - [(s_{21} + \mathcal{D}_3 s_{12}) + \mathcal{D}_3 \mathcal{D}_3 (s_{31} + \mathcal{D}_2 s_{13})] \\ &\quad + \frac{1}{2} [\mathcal{D}_2 \mathcal{D}_2 \mathcal{D}_3 \mathcal{D}_3 (\tau_{21} - \tau_{31}) - \mathcal{D}_3 \mathcal{D}_3 (\tau_{21} - \tau_{31}) - \mathcal{D}_2 \mathcal{D}_2 (\tau_{21} - \tau_{31}) + (\tau_{21} - \tau_{31})] \end{aligned} \quad (22)$$

As pointed out in [17] and [12], equation (21) shows that  $X$  is the difference of two sums of phase measurements, each corresponding to a specific light path from a laser onboard spacecraft 1 having phase noise  $\phi_1$ . The first square-bracket term in equation (21) represents a synthesized light-beam transmitted from spacecraft 1 and made to bounce once at spacecraft 3 and 2 respectively. The second square-bracket term instead corresponds to another beam also originating from the same laser, experiencing the same overall delay as the first beam, but bouncing off spacecraft 2 first and then spacecraft 3. When they are recombined they will cancel the laser phase fluctuations exactly, having both experienced the same total delays.

### III. TIME-DELAY INTERFEROMETRY WITH MOVING SPACECRAFT

The rotational motion of the LISA array results in a difference of the light travel times in the two directions around a Sagnac circuit [14],[15]. Two time delays along each arm must be used, say  $L'_i$  and  $L_i$  for clockwise or counterclockwise propagation as they enter in any of the TDI combinations. Furthermore, since  $L_i$  and  $L'_i$  not only differ from one another but can be time dependent (they "flex"), it was shown that the "first generation" TDI combinations do not completely cancel the laser phase noise (at least with present laser stability requirements), which can enter at a level above the secondary noises. For LISA, and assuming  $\dot{L}_i \simeq 10\text{m/sec}$  [18], the estimated magnitude of the remaining frequency fluctuations from the laser can be about 30 times larger than the level set by the secondary noise sources in the center of the frequency band. In order to solve this potential problem, it has been shown that there exist new TDI combinations that are immune to first order shearing (flexing, or constant rate of change of delay times). These combinations can be derived by using the time-delay operators formalism introduced in the previous section, although one has to keep in mind that now these operators no longer commute [13].

In order to derive the new, "flex-free" TDI combinations we will start by taking specific combinations of the one-way data in such a way so as to retain only one of the three noises  $\phi_i, i = 1, 2, 3$  if possible. In this way we can then implement an iterative procedure based on the use of these basic combinations and of time-delay operators, to cancel the laser noises after dropping terms that are quadratic in  $\dot{L}/c$  or linear in the accelerations. This iterative time-delay method, to first order in the velocity, is illustrated abstractly as follows. Given a

function of time  $\Psi = \Psi(t)$ , time delay by  $L_i$  is now denoted either with the standard comma notation [9] or by applying the delay operator  $\mathcal{D}_i$  introduced in the previous section

$$\mathcal{D}_i \Psi = \Psi_{,i} \equiv \Psi(t - L_i(t)) . \quad (23)$$

We then impose a second time delay  $L_j(t)$ :

$$\begin{aligned} \mathcal{D}_j \mathcal{D}_i \Psi &= \Psi_{,ij} \equiv \Psi(t - L_j(t) - L_i(t - L_j(t))) \\ &\simeq \Psi(t - L_j(t) - L_i(t) + \dot{L}_i(t)L_j) \\ &\simeq \Psi_{,ij} + \dot{\Psi}_{,ij} \dot{L}_i L_j . \end{aligned} \quad (24)$$

A third time delay  $L_k(t)$  gives:

$$\begin{aligned} \mathcal{D}_k \mathcal{D}_j \mathcal{D}_i \Psi &= \Psi_{,ijk} = \Psi(t - L_k(t) - L_j(t - L_k(t)) - L_i(t - L_k(t) - L_j(t - L_k(t)))) \\ &\simeq \Psi_{,ijk} + \dot{\Psi}_{,ijk} [\dot{L}_i(L_j + L_k) + \dot{L}_j L_k] , \end{aligned} \quad (25)$$

and so on, recursively; each delay generates a first-order correction proportional to its rate of change times the sum of all delays coming after it in the subscripts. Commas have now been replaced with semicolons [12], to remind us that we consider moving arrays. When the sum of these corrections to the terms of a data combination vanishes, the combination is called flex-free.

Also, note that each delay operator,  $\mathcal{D}_i$ , has a unique inverse,  $D_i^{-1}$ , whose expression can be derived by requiring that  $D_i^{-1} \mathcal{D}_i = I$ , and neglecting quadratic and higher order velocity terms. Its action on a time series  $\Psi(t)$  is

$$D_i^{-1} \Psi(t) \equiv \Psi(t + L_i(t + L_i)) . \quad (26)$$

Note that this is not like an advance operator one might expect, since it advances not by  $L_i(t)$  but rather  $L_i(t + L_i)$ .

### A. The Unequal-Arm Michelson

The unequal-arm Michelson combination relies on the four measurements  $\eta_1$ ,  $\eta_{1*}$ ,  $\eta_{2*}$ , and  $\eta_3$ . Note that the two combinations  $\eta_1 + \eta_{2*,3}$ ,  $\eta_{1*} + \eta_{3,2'}$  represent the two synthesized two-way data measured onboard spacecraft 1, and can be written in the following form

$$\eta_1 + \eta_{2*,3} = (\mathcal{D}_3 \mathcal{D}_{3'} - I) \phi_1 , \quad (27)$$

$$\eta_{1*} + \eta_{3,2'} = (\mathcal{D}_{2'} \mathcal{D}_2 - I) \phi_1 , \quad (28)$$

where  $I$  is the identity operator, and we have also used interchangeably the comma notation. Since in the stationary case any pairs of these operators commute, i.e.  $\mathcal{D}_i \mathcal{D}_{j'} - \mathcal{D}_{j'} \mathcal{D}_i = 0$ , from equations (27, 28) it is easy to derive the following expression for the unequal-arm interferometric combination,  $X$ , which eliminates,  $\phi_1$

$$X = [\mathcal{D}_{2'} \mathcal{D}_2 - I] (\eta_1 + \eta_{2',3}) - [(\mathcal{D}_3 \mathcal{D}_{3'} - I)] (\eta_{1*} + \eta_{3,2'}). \quad (29)$$

If, on the other hand, the time-delays depend on time, the expression of the unequal-arm Michelson combination above no longer cancels  $\phi_1$ . In order to derive the new expression for the unequal-arm interferometer that accounts for “flexing”, let us first consider the following two combinations of the one-way measurements entering into the  $X$  observable given in equation (29):

$$[(\eta_{1*} + \eta_{3,2'}) + (\eta_1 + \eta_{2',3})_{;22'}] = [D_{2'} D_2 D_3 D_{3'} - I] \phi_1, \quad (30)$$

$$[(\eta_1 + \eta_{2',3}) + (\eta_{1*} + \eta_{3,2'})_{;3'3}] = [D_3 D_{3'} D_2 D_2 - I] \phi_1. \quad (31)$$

Using equations (30, 31) we can use the delay technique to finally derive the following expression for the new unequal-arm Michelson combination  $X_1$  that accounts for the flexing effect,

$$\begin{aligned} X_1 = & [D_2 D_{2'} D_3 D_3 - I] [(\eta_{21} + \eta_{12,3'}) + (\eta_{31} + \eta_{13,2})_{;33'}] \\ & - [D_{3'} D_3 D_2 D_{2'} - I] [(\eta_{31} + \eta_{13,2}) + (\eta_{21} + \eta_{12,3'})_{;2'2}]. \end{aligned} \quad (32)$$

This expression is readily shown to be laser-noise-free to first order of spacecraft separation velocities  $\dot{L}_i$ : it is “flex-free”. As usual,  $X_2$  and  $X_3$  are obtained by cyclic permutation of the spacecraft indices.

The reader is referred to [12], [13] for a derivation of all the other TDI combinations valid for the non-stationary LISA configuration.

#### IV. TIME-DELAY INTERFEROMETRIC RANGING (TDIR)

In the case of a stationary LISA spacecraft array, it was estimated [19] that the time delays need to be known with an accuracy of about 100 ns, if the various TDI combinations are to work effectively, suppressing the residual laser phase fluctuations to a level below the secondary noises (such as the proof-mass and optical-path noises). For an array

of spacecraft in relative motion along realistic Solar orbits, the more complicated (*second-generation*) TDI combinations require an even more accurate knowledge of the time delays [20]. The most direct implementation of TDI consists in triggering the phase measurements at the correct delayed times (within the required accuracy), as suggested in Ref. [19]. This approach requires the real-time, onboard knowledge of the light-travel times between pairs of spacecraft, which determine the TDI time delays. Although the triggering approach is feasible in principle, it complicates the design of the optical phasemeter system, and it requires an independent onboard ranging capability. Recently, it was pointed out [21] that the phase measurements at the specific times needed by the TDI algorithm can be computed *in post-processing* with the required accuracy, by the fractional-delay interpolation (FDI) [21, 22] of regularly sampled data (with a sampling rate of 10 Hz for a GW measurement band extending to 1 Hz). This implies that it is then possible to implement numerically a variational procedure to determine the TDI time delays from the phase-difference measurements themselves, eliminating the need for an independent onboard ranging capability. Since this variational procedure relies on the TDI combinations, it has been named Time-Delay Interferometric Ranging (TDIR).

In conventional spacecraft ranging either one-way or two-way delay times are measured. In one-way ranging, for instance, two or more tones are coherently modulated onto the transmitted carrier and their phases are measured at the receiver. By then further differencing and dividing them by the spanned bandwidth one gets the group delay and hence the time delay (up to an ambiguity of  $c$  divided by the spanned bandwidth of the ranging tones). In two-way ranging instead a known ranging code is modulated on the transmitted carrier, transponded by a distant spacecraft back to the originator, and the received signal is then cross-correlated with the ranging code to determine the two-way time of flight.

TDIR differs from these methods in that it uses the unmodulated laser noises in a three-element array, which are canceled in TDI combinations assembled with the correct inter-spacecraft light-travel times. This means that TDI can be used to estimate the light-travel times by minimizing the laser noise power in the TDI combinations as a function of the postulated light-travel times: this process defines TDIR. As an example of how TDIR works, we shall consider again the second-generation TDI combinations  $X_1$  derived above. Note,

however, that that expression should now be rewritten in the following form

$$\begin{aligned}
X_1 = & [D_2 D_{2'} D_{\hat{3}} D_{\hat{3}'} - I] [(\eta_{21} + \eta_{12;\hat{3}'}) + (\eta_{31} + \eta_{13;\hat{2}})_{;\hat{3}\hat{3}'}] \\
& - [D_{\hat{3}} D_{\hat{3}'} D_2 D_{2'} - I] [(\eta_{31} + \eta_{13;\hat{2}}) + (\eta_{21} + \eta_{12;\hat{3}'})_{;\hat{2}'\hat{2}}]. \quad (33)
\end{aligned}$$

The time-delay indices that appear in Eq. (33) with a hat need to be provided by the data analyst (or, in the triggering approach, by the onboard ranging subsystem) with the accuracy required for effective laser noise cancellation. Thus, the  $X_1$ -based implementation of TDIR works by *minimizing the power in  $X_1$  with respect to the hatted delays  $\hat{L}_k$* . Since the TDI combinations constructed with the actual delays cancel laser phase noise to a level  $10^8$  below the secondary noises [12], it follows that if we neglect all non-laser sources of phase noise affecting the  $X_1$  combination, the minimum of the power integral

$$I^{(0)}(\hat{L}_k) = \frac{1}{T} \int_0^T [X_1^{(0)}(\hat{L}_k)]^2 dt \quad (34)$$

will occur for  $\hat{L}_k = L_k$  (with  $k = 1, 2, 3, 1', 2', 3'$ ; here the superscript  $(0)$  denotes *laser-noise-only* quantities). The search for this minimum can be implemented in post processing, using FDI [21] to generate the needed  $s_{ij}$  and  $\tau_{ij}$  samples at the delayed times corresponding to any choice of the  $\hat{L}_k$ .

In reality, the presence of non-laser phase noises (possibly including GWs) will displace the location of the minimum from  $L_k$ . Writing  $X_1 = X_1^{(0)} + X_1^{(n)}$  (with  $X_1^{(n)}$  obtained by setting all  $\phi_i, \phi_i^*$  to zero), the power integral becomes

$$I^{(n)}(\hat{L}_k) = \frac{1}{T} \int_0^T [X_1(\hat{L}_k)]^2 dt, \quad (35)$$

or explicitly,

$$\begin{aligned}
I^{(n)}(\hat{L}_k) = & I^{(0)}(\hat{L}_k) + \frac{1}{T} \int_0^T [X_1^{(n)}]^2 dt \\
& + \frac{2}{T} \int_0^T X_1^{(n)} X_1^{(0)}(\hat{L}_k) dt. \quad (36)
\end{aligned}$$

Here we have written the non-laser phase noise  $X_1^{(n)}$  as independent of the delays  $\hat{L}_k$ : this holds true for a search conducted sufficiently close to the true minimum, since the  $\phi_i, \phi_i^*$  are much larger than the secondary noises, and so are their variations. The minimum of  $I^{(n)}(\hat{L}_k)$  can be displaced from  $\hat{L}_k = L_k$  because the third term of Eq. (35) [the cross-correlation integral of  $X_1^{(n)}$  and  $X_1^{(0)}(\hat{L}_k)$ ] can be negative and offset a concurrent increase in  $I^{(0)}(\hat{L}_k)$ . The achievable time-delay accuracies will depend on the level of the residual laser

noise, the levels of the secondary noises in  $X_1$ , and the integration time  $T$ . We expect the arm-length errors to be determined by the interplay of the first and third terms in Eq. (36). By equating the variance from the imperfect cancellation of the laser with the estimation-error variance of the cross-term in Eq. (36), we can roughly estimate how well the time delays will be determined with TDIR:  $\delta L_k \sim (\sigma_{X_1^{(n)}}/\sigma_{\dot{X}_1^{(0)}}) \sqrt{\rho/T}$ , where  $\sigma_{X_1^{(n)}}$  and  $\sigma_{\dot{X}_1^{(0)}}$  are the root-mean-squares of the secondary noises and of the time derivative of the laser noise in  $X_1$ , and  $\rho$  is the temporal width of the secondary-noise autocorrelation function. For nominal LISA noises and  $T \simeq 10,000$  s we thus expect  $\delta L_k$  of 30 ns or better to be achievable.

The TDIR concept described above was simulated, for a realistic model of the LISA orbits and instruments, with the *Synthetic LISA* software package [23]. The simulation included the generation of a number of *chunks* of contiguous data for the  $s_{ij}$  and  $\tau_{ij}$  measurements, sampled at intervals of 0.25 s, and containing pseudo-random laser, proof-mass, and optical-path noises at the nominal level set by the LISA pre-phase A specification [4, 23]. The data durations considered were 8,192, 16,384, and 32,768 s.

The 18 noise processes (corresponding to the six lasers, proof masses, and optical paths) were assumed to be uncorrelated, Gaussian, and stationary, with (respectively) white,  $f^{-2}$ , and  $f^2$  PSDs, band-limited at 1 Hz. The frequency-fluctuation measurements contained also the responses due to GWs from two circular binaries with  $f_{\text{GW}} \simeq 1$  and 3 mHz, located respectively at the vernal equinox and at ecliptic latitude  $45^\circ$  and longitude  $120^\circ$ . The strength of the two sources was adjusted to yield an optimal S/N of  $\sim 500$  over a year (for  $X_1$ ), guaranteeing that there will be times of the year when each source will be clearly visible above the noise in an observation time  $\sim 10,000$  s.

By putting the three LISA spacecraft on realistic trajectories, the resulting time and direction dependence [12] of the light travel times can be written in the following form [23, 24]

$$L_k(t) = L + \frac{1}{32}(eL) \sin(3\Omega t - 3\xi_0) - \left[ \frac{15}{32}(eL) \pm (\Omega RL) \right] \sin(\Omega t - \lambda_k), \quad (37)$$

where the plus (minus) refers to unprimed (primed) indices. In Eq. (37)  $L/c \simeq 16.68$  s is the average light travel time, and

$$(\lambda_1, \lambda_2, \lambda_3) = \left( \xi_0, \xi_0 + \frac{4\pi}{3}, \xi_0 + \frac{2\pi}{3} \right), \quad (38)$$

with  $\xi_0$  an arbitrary constant (set to 0 in our simulations) giving the phase of the spacecraft motion around the guiding center of the LISA array. The starting times of the chunks were spread across a year to sample the time dependence of the  $L_k$  and the directionality of the GW responses.

Separately for each chunk, we minimized  $I^{(n)}[\hat{L}_k(t)]$  [Eq. (35)] starting from guesses for the  $\hat{L}_k$  affected by errors  $\gtrsim 50$  km/c, very much larger than typical accuracy of radio tracking from Earth [18]. The minimization was carried out using a Nelder–Mead simplex-based algorithm [25]. The effective cancellation of laser noise with TDI requires modeling the time dependence of the travel times *within* the chunks. In our simulations, we used two such models:

1. An orbital-dynamics model (ODM) given by Eq. (37), with  $\widehat{eL}$ ,  $\widehat{\Omega RL}$ , and  $\widehat{\xi}_0$  taken as the independent search parameters with respect to which  $I^{(n)}$  is minimized. We excluded  $L$  and  $\Omega$  from the search because the dependence of the  $L_k(t)$  on such an extended parameter set is degenerate on time-scales  $\sim 10,000$  s.
2. A linear model (LM) given by  $\hat{L}_k(t) = \hat{L}_k^0 + \hat{L}_k^1(t - t_0)$  [with  $t_0$  set to the beginning of each chunk]. Because the expression for  $X_1$  does not contain the travel times  $L_1$  and  $L_{1'}$ , our independent search parameters are the constants  $\hat{L}_k^0$  and  $\hat{L}_k^1$  for  $k = 2, 2', 3, 3'$  (eight numbers altogether).

Figures 4 and 5 show the results of our simulations. The average travel-time errors  $\Delta L$  displayed in Fig. 4 are defined as  $\Delta L = (\Delta L_2 + \Delta L_{2'} + \Delta L_3 + \Delta L_{3'})/4$ , with

$$\Delta L_k = \sqrt{\frac{1}{T} \int_{t_0}^{t_0+T} (\hat{L}_k(t) - L_k(t))^2 dt}. \quad (39)$$

Because the noises have different realizations in each chunk and because the local behavior of the  $L_k(t)$  [Eq. (37)] changes along the year, the average error  $\Delta L$  of each chunk is a random variable. Its distribution is approximated by the histograms of Fig. 4, which refer to populations of respectively 512 (for  $T = 8,192$  s), 256 (for  $T = 16,384$  s), and 128 (for  $T = 32,768$  s) chunks (hence the roughness of the curves).

It turns out that the linear model is not quite sufficient to model the changes of the time-delays during the chunk lengths considered, since the *minimum*  $\Delta L$ s [computed by least-squares fitting the parameters  $\hat{L}_k^0$  and  $\hat{L}_k^1$  to the  $L_k(t)$ ] are in the range 0.25–2.60 m

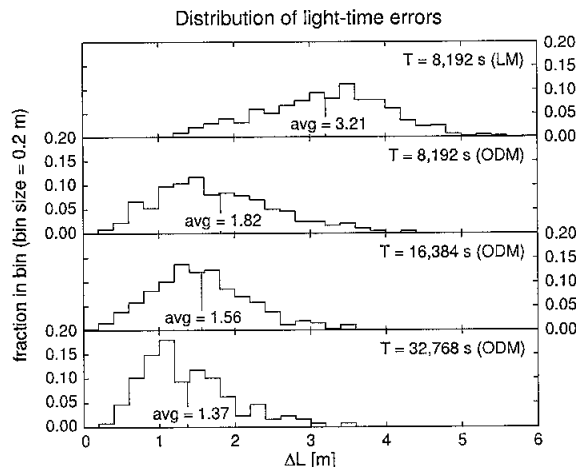


FIG. 4: Distribution of errors  $\Delta L$  [see Eq. (39) and the main text above it] in the determination of light travel times, using  $X_1$ -based TDIR with chunk durations of 8,192 s (for the LM and ODM models), and 16,384 and 32,768 s (for the ODM model only). As expected, the errors are lower for longer integration times  $T$ ; for the LM model, the larger errors are due to the unmodeled curvature in the time dependence of the light-travel times. The distributions shown correspond to samples of 512, 256, and 128 chunks for  $T = 8,192, 16,384,$  and  $32,768$  s respectively, spread across a year.

(for  $T = 8,192$  s), 1–10 m (for  $T = 16,384$  s), and 4–40 m (for  $T = 32,768$  s). Thus, in Figs. 4 and 5 we show results only for the linear model with  $T = 8,192$  s. [The minimization of  $I^{(n)}$  over the LM parameters is delicate, because for  $X_1$  the laser-noise residuals turn out to depend strongly on  $\Delta L_2$ ,  $\Delta L_{3'}$ , and  $\Delta L_{2'} - \Delta L_3$ , but only weakly on  $\Delta L_{2'} + \Delta L_3$ . In this case, the Nelder–Mead algorithm can be made to return accurate results by using the search parameters  $\hat{L}_2^0$ ,  $\hat{L}_{3'}^0$ ,  $\widehat{L_{2'} - L_3^0}$ , and  $\widehat{L_{2'} + L_3^0}$ , plus the corresponding  $\hat{L}_k^1$  parameters.]

Figure 5 shows the spectra of the *residual* laser noise [i.e., of  $X_1^{(0)}$  at the minimum of  $I^{(n)}(\hat{L}_k)$ ], as compared with spectra of GWs and secondary noises [i.e., of  $X_1^{(n)}$ ]. The spectra are computed separately for each chunk using triangle-windowed periodograms, and then averaged over the chunk populations. The two GW sources stand clearly above the secondary noises at 1 and 3 mHz. We see that the TDI cancellation of laser noise with TDIR-determined time-delays is essentially complete, with the residual laser noise several orders of magnitude below the secondary noises. We conclude that for  $T \sim 10,000$  s, with the nominal LISA noises, and even in the presence of very strong GW signals, TDIR can easily reach the time-delay accuracy required for second-generation TDI. For frequencies below 10

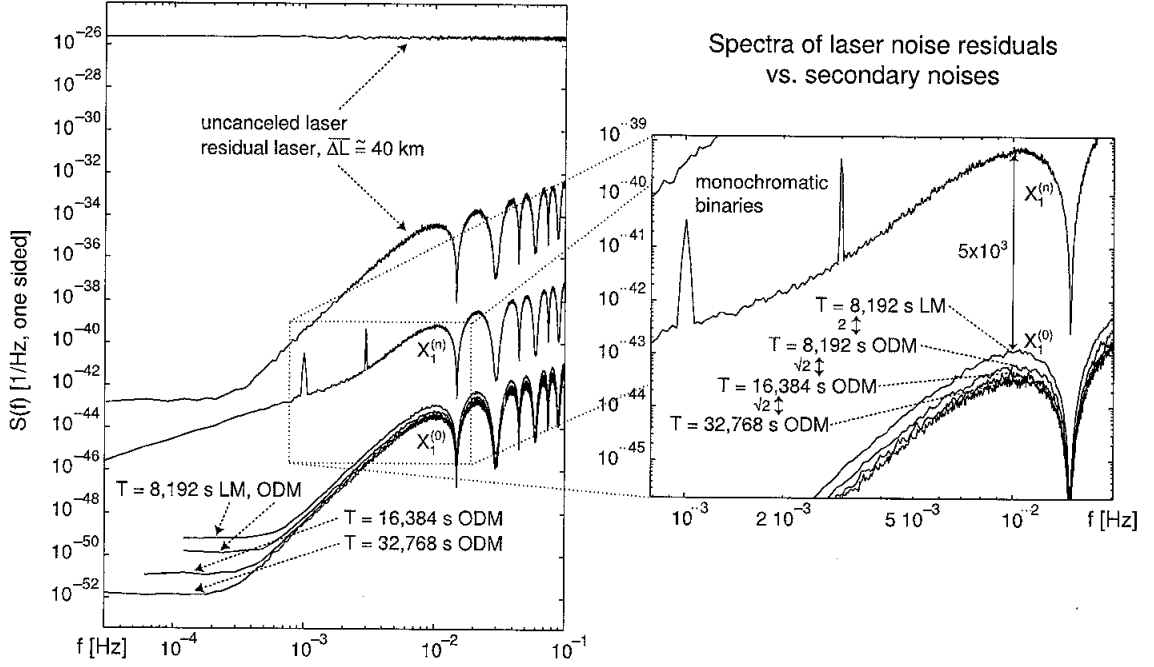


FIG. 5: Spectra of frequency laser noise (bottom curves) and of GW plus secondary noises (top curve) at the end of TDIR minimization using chunk durations of 8,192 s (for the LM and ODM models), and 16,384 and 32,768 s (for the ODM model only). We show averages of the spectra computed separately for each chunk using a triangle-windowed periodogram; the averages are taken over populations of 512, 256, and 128 chunks for  $T = 8,192$ , 16,384, and 32,768 s respectively, spread across a year. In all cases, laser noise is suppressed to levels several orders of magnitude below the secondary noises: the cutout graph on the right shows that the typical laser-noise suppression factor with respect to secondary noise is  $\sim 5 \times 10^3$  for the worst case considered (8,192-s LM); it improves by a factor  $\sim 2$  for 8,192-s ODM, and by factors of  $\sim \sqrt{2}$  for each successive doubling of  $T$ . The GWs from the two circular binaries stand clearly above the noise at 1 and 3 mHz.

mHz, the residual laser-noise power decays as  $f^6$ , while the secondary noises decrease only as  $f^2$ . We attribute the flattening near 0.1 mHz (which is insignificant with respect to the LISA performance) to a combination of leakage and aliasing in the numerical estimation of the spectra and of real effects due to the first non-constant terms in the travel time errors across the chunks.

Finally, we estimated the power in the Fourier bins containing the simulated signals using two different time series: in the first  $X_1$  was formed using perfectly known time delays, in

the second using the TDIR-determined time delays. Analyzing the 32,768-s chunks at the times along the simulated year where the signal amplitudes were maximum, we find that the signal powers in the two time series agree to the numerical precision of the calculation (about a part in  $10^5$ ).

From figures (4,5) we conclude that, for the nominal LISA noises, integration times  $\sim 10,000$  s, TDIR determines the time delays with accuracies sufficient to suppress the laser phase fluctuations to a level below the LISA secondary noises, while at the same time preserving GW signals. Our simulations assumed synchronized clocks aboard the spacecraft, but we anticipate that TDIR may be extended to achieve synchronization, by minimizing noise power also with respect to clock parameters.

TDIR has the potential of simplifying the LISA design, allowing the implementation of TDI without a separate inter-spacecraft ranging subsystem. At the very least, TDIR can supplement such a subsystem, allowing the synthesis of TDI combinations during ranging dropouts or glitches. TDIR may be applicable in other forthcoming space science missions that rely on spacecraft formation flying and on inter-spacecraft ranging measurements to achieve their science objectives.

### Acknowledgement

I would like to thank my JPL collaborators and friends, Frank B. Estabrook, John W. Armstrong, and Michele Vallisneri for all the stimulating conversations I had with them on the material presented in this paper. This research was performed at the Jet Propulsion Laboratory, California Institute of Technology, under contract with the National Aeronautics and Space Administration.

- 
- [1] M. Tinto, and F.B. Estabrook, *Phys. Rev. D*, **52**, 1749, (1995).
  - [2] M. Tinto, *Class. Quantum Grav.*, **19**, 7, 1767 (2002).
  - [3] F.B. Estabrook, and H.D. Wahlquist, *Gen. Relativ. Gravit.* **6**, 439 (1975).
  - [4] LISA: (Laser Interferometer Space Antenna) *An international project in the field of Fundamental Physics in Space*, Pre-Phase A Report, **MPQ 233**, (Max-Planck-Institute für Quantenoptic, Garching bei München, 1998).

- [5] Wei-Tou Ni, This Volume.
- [6] M. Tinto, and J.W. Armstrong *Phys. Rev. D*, **59**, 102003 (1999).
- [7] M. Tinto, F.B. Estabrook, and J.W. Armstrong, *Phys. Rev. D*, **65**, 082003 (2002).
- [8] M. Tinto, *Phys. Rev. D*, **58**, 102001, (1998).
- [9] J.W. Armstrong, and F.B. Estabrook, & M. Tinto, *ApJ*, **527**, 814 (1999).
- [10] S.V. Dhurandhar, K. R. Nayak, and J.-Y. Vinet *Phys. Rev. D*, **65**, 102002 (2002)
- [11] F.B. Estabrook, M. Tinto, and J.W. Armstrong, *Phys. Rev. D*, **62**, 042002 (2000).
- [12] D.A. Shaddock, M. Tinto, F.B. Estabrook, and J.W. Armstrong, *Phys. Rev. D*, **68**, 061303 (2003).
- [13] M. Tinto, F.B. Estabrook, and J.W. Armstrong, *Phys. Rev. D*, **69**, 082001, (2004).
- [14] D.A. Shaddock, *Phys. Rev. D*, **69**, 022001 (2004).
- [15] N.J. Cornish & R.W. Hellings, *Class. Quantum Grav.*, **20**, 4851, (2003).
- [16] M. Tinto, M. Vallisneri, and J.W. Armstrong, *Phys. Rev. D*, **71**, 041101(R) (2005).
- [17] D. Summers, "Algorithm tradeoffs," oral presentation, 3rd progress meeting of the ESA funded LISA PMS Project. ESTEC, NL, February 2003.
- [18] W.M. Folkner, F. Hechler, T.H. Sweetser, M.A. Vincent, and P.L. Bender, *Clas. Quantum Grav.*, **14**, 1543, (1997).
- [19] M. Tinto, D. A. Shaddock, J. Sylvestre, and J. W. Armstrong, *Phys. Rev. D* **67**, 122003 (2003).
- [20] M. Vallisneri, M. Tinto, and J. W. Armstrong, in preparation (2004).
- [21] D. A. Shaddock, B. Ware, R. E. Spero, and M. Vallisneri, *Phys. Rev. D*, **70**, 081101 (2004).
- [22] T. I. Laakso et al., *IEEE Signal Processing Magazine* **13**, 30 (1996).
- [23] M. Vallisneri, *Phys. Rev. D*, **71**, 022001 (2005).
- [24] N. Cornish and L. Rubbo, *Phys. Rev. D* **67**, 022001 (2003).
- [25] J. A. Nelder and R. Mead, *Computer Journal* **7**, 308 (1965).